Adaptive morphological filters based on a multiple orientation vector field dependent on image local features

Álvar-Ginés Legaz-Aparicio[1], Rafael Verdú-Monedero[1], Jesús Angulo[2]

[1] *Universidad Politécnica de Cartagena, Cartagena, 30202, Spain*
[2] *MINES ParisTech, PSL-Research University, CMM-Centre de Morphologie Mathématique, France*

Abstract

This paper addresses the formulation of adaptive morphological filters based on spatially-variant structuring elements. The adaptivity of these filters is achieved by modifying the shape and orientation of the structuring elements according to a multiple orientation vector field. This vector field is provided by means of a bank of directional openings which can take into account the possible multiple orientations of the contours in the image. After reviewing and formalizing the definition of the spatially-variant dilation, erosion, opening and closing, the proposed structuring elements are described. These spatially-variant structuring elements are based on ellipses which vary over the image domain adapting locally their orientation according to the multiple orientation vector field and their shape (the eccentricity of the ellipses) according to the distance to relevant contours of the objects. The proposed adaptive morphological filters are used on gray-level images and are compared with spatially-invariant filters, with spatially-variant filters based on a single orientation vector field, and with adaptive morphological bilateral filters. Results show that the morphological filters based on a multiple orientation vector field are more adept at enhancing and preserving structures which contains more than one orientation.

Keywords: Mathematical morphology, adaptive morphology, adaptive structuring elements, spatially-variant structuring elements

1. Introduction

Mathematical morphology is a nonlinear image processing methodology useful for solving efficiently many image analysis tasks [1]. From a mathematical point of view, it is based on two basic operators, dilation and erosion, which correspond respectively to the convolution in the max-plus algebra and its dual convolution. More precisely, in Euclidean (translation invariant) mathematical morphology, the pair of adjoint and dual operators dilation (sup-convolution) $(f \oplus b)(x)$ and erosion (inf-convolution) $(f \ominus b)(x)$ of an image $f : E \subset \mathbb{R}^n \to \overline{\mathbb{R}} = \mathbb{R} \cup \{-\infty, +\infty\}$ are given by [2, 3]:

$$\begin{cases} \delta_b(f)(x) = (f \oplus b)(x) = \sup_{y \in E} \{f(y) + b(y - x)\}, \\ \varepsilon_b(f)(x) = (f \ominus b)(x) = \inf_{y \in E} \{f(y) - b(y + x)\}, \end{cases} \tag{1}$$

where $b : \mathbb{R}^n \to \overline{\mathbb{R}}$ is the structuring function which determines the effect of the operator. The structuring function plays a similar role to the kernel in classical linear filtering using convolution. By allowing infinity values, the further convention for ambiguous expressions should be considered: $f(y) + b(x - y) = -\infty$ when $f(y) = -\infty$ or $b(x - y) = -\infty$, and that $f(y) - b(y + x) = +\infty$ when $f(y) = +\infty$ or $b(y + x) = -\infty$. We easily note that both are invariant under translations (i.e., commute with the translation operator) in the spatial ("horizontal") space E and in the image intensity ("vertical") space $\overline{\mathbb{R}}$, i.e.,

$$f(x) \mapsto f_{(y,\alpha)}(x) = f(x - y) + \alpha, \tag{2}$$

with $y \in E$ and $\alpha \in \overline{\mathbb{R}}$, then

$$\delta_b(f_{(y,\alpha)})(x) = \delta_b(f)(x - y) + \alpha. \tag{3}$$

The structuring function is typically a parametric family $b_t(x)$, where $t > 0$ is the scale parameter. In particular, the canonical structuring function is the paraboloidal shape (i.e., square of the Euclidean distance) [4, 5]:

$$p_t(x) = -\frac{\|x\|^2}{2t}. \tag{4}$$

Due to its properties of semigroup, dimension separability and invariance to transform domain, the structuring function $p_t(x)$ plays a similar role to the Gaussian kernel in (linear) covolution-based filtering. The corresponding quadratic dilation and erosion by $p_t(x)$ are related to the following initial-value Hamilton–Jacobi first-order partial differential equation (Hamilton-Jacobi PDE) [6, 7]:

$$\begin{cases} \frac{\partial u}{\partial t} = \pm\frac{1}{2}\|\nabla u\|^2, & x \in \mathbb{R}^n, \ t > 0 \\ \\ u(x,0) = f(x), & x \in \mathbb{R}^n \end{cases} \tag{5}$$

This Hamilton–Jacobi PDE does not admit classic (i.e., everywhere differentiable) solutions but can be studied in the framework of the theory of viscosity solutions [8]. It is well known that the solutions of the Cauchy problem (5) are given by the so-called Hopf–Lax–Oleinik formulas [9], for + sign and − sign, respectively:

$$u(x,t) = \sup_{y\in\mathbb{R}^n}\left\{f(y) - \frac{\|x-y\|^2}{2t}\right\} = (f \oplus p_t)(x) \quad \text{(for + sign)}, \tag{6}$$

$$u(x,t) = \inf_{y\in\mathbb{R}^n}\left\{f(y) + \frac{\|x-y\|^2}{2t}\right\} = (f \ominus p_t)(x) \quad \text{(for − sign)}. \tag{7}$$

Such PDE model is fundamental to continuous mathematical morphology, and research on numerical schema for the solution of spatially-variant counterparts of (5) is still active [10].

The theory of morphological filtering is based on the opening $(f \circ b)(x)$ and closing $(f \bullet b)(x)$ operators, obtained respectively by the composition product of erosion-dilation and dilation-erosion using the same structurig function, i.e.,

$$\begin{cases} \gamma_b(f)(x) = (f \circ b)(x) = ((f \ominus b) \oplus b)(x) = \sup_{z\in E}\inf_{y\in E}\{f(y) - b(y-z) + b(z-x)\}, \\ \varphi_b(f)(x) = (f \bullet b)(x) = ((f \oplus b) \ominus b)(x) = \inf_{z\in E}\sup_{y\in E}\{f(y) + b(z-y) - b(x-z)\}. \end{cases} \tag{8}$$

In order to have a better insight of the effect of the opening and the closing of a function, let us rewrite $(f \circ b)(x)$ as follows:

$$\gamma_b(f) = \bigvee\left\{b_{(y,\alpha)} \mid (y,\alpha) \in E \times \overline{\mathbb{R}}, \ b_{(y,\alpha)} \leq f\right\}, \tag{9}$$

where $\bigvee$ denotes the supremum. Therefore, in the product space $E \times \overline{\mathbb{R}}$ the subgraph of the opening is generated by the upper envelope of the horizontally and vertically translated shape function $b(x-y) + \alpha$ under the function f. In other words, function $(f \circ b)(x)$ can be seen as the supremum of the invariants parts of f under-swept by b. Regarding the closing $(f \bullet b)(x)$, a similar geometric dual interpretation is obtained:

$$\varphi_b(f) = \bigwedge\left\{\check{b}_{(y,\alpha)} \mid (y,\alpha) \in E \times \overline{\mathbb{R}}, \ \check{b}_{(y,\alpha)} \geq f\right\}, \tag{10}$$

where $\bigwedge$ denotes the infimum and $\check{b}(x) = -b(-x)$. This expression corresponds to the invariant parts of f over-swept by the horizontally and vertically symmetric structuring function $\check{b}$. From (9), it is straightforward to see that the opening is (i) increasing, (ii) idempotent and (iii) anti-extensive, i.e., $\forall x$, (i) $f(x) \leq g(x) \Rightarrow \gamma_b(f)(x) \leq \gamma_b(g)(x)$; (ii) $\gamma_b(\gamma_b(f)) = \gamma_b(f)$; and (iii) $\gamma_b(f)(x) \leq f(x)$. From (10), the closing is increasing and idempotent, but being extensive: $\varphi_b(f)(x) \geq f(x)$, $\forall x$. More complex filters can be obtained by composition of openings and closings [2, 3].

At this point, it could be interesting for a general reader to compare these morphological operators to the most extended family of filters based on the standard convolution of a function f by a translation-invariant kernel k:

$$(f * k)(x) = \int_E f(y)k(y-x)dy, \tag{11}$$

and in particular, to the case of canonical kernel in linear filtering, the so-called Gaussian kernel at scale t:

$$(f * g_t)(x) = C \int_E f(y) \exp\left(-\frac{\|x-y\|^2}{2t}\right) dy, \quad C = (2\pi t)^{-n/2}. \tag{12}$$

One can easily identify that the quadratic dilation (resp. erosion) is just a convolution in a max-plus (resp. min-minus) algebra instead of the plus-times algebra, and $p_t(x)$ is, up to the constant C, just the logarithm of $g_t(x)$. However, we point out that the parallelism with the quadratic opening is more relevant:

$$(f \circ p_t)(x) = \bigvee_{y \in E, \alpha \in \overline{\mathbb{R}}} \left\{ -\frac{\|x-y\|^2}{2t} + \alpha \ : \ -\frac{\|x-y\|^2}{2t} + \alpha \leq f \right\}. \tag{13}$$

Thus, the standard regularization of the function by a Gaussian kernel weighted-average in $(f * g_t)$ is replaced in $(f \circ p_t)(x)$ by a maximal quadratic under-regularization, or an minimal over-regularization in $(f \bullet p_t)$.

The most commonly studied framework, which additionally presents better properties of invariance, is based on flat structuring functions, called structuring elements. More precisely, let B be a Boolean set defined at the origin, i.e., $B \subseteq E$ or $B \in \mathcal{P}(E)$, which defines the "shape" of the structuring element, the associated structuring function is given by

$$b(x) = \begin{cases} 0 & \text{if } x \in B, \\ -\infty & \text{if } x \in B^c, \end{cases} \tag{14}$$

where B^c is the complement set of B in $\mathcal{P}(E)$. Hence, the flat dilation $(f \oplus B)$ and flat erosion $(f \ominus B)$ can be computed respectively by the moving local maxima and minima filters, i.e.,

$$\begin{cases} \delta_B(f)(x) = (f \oplus B)(x) = \sup_{y \in B} \{f(x-y)\} = \bigvee_{y \in B} f(x-y), \\ \varepsilon_B(f)(x) = (f \ominus B)(x) = \inf_{y \in B} \{f(x+y)\} = \bigwedge_{y \in B} f(x+y). \end{cases} \tag{15}$$

A detailed presentation of the principles and applications of morphological image analysis is provided in [1]. Recently, in [11], the state of the art in mathematical morphology is exposed in a didactic fashion, with original and novel content.

Traditionally, structuring functions (resp. structuring elements) have been space translation-invariant, applying the function b (or the same set B, i.e., same shape and orientation) in all pixels of the image. In the last years, the notion of adaptive morphological operators [12] based on using adaptive structuring elements, which change their shape and orientation over the space E, according to the local image features, have been proposed. In [13] an overview of adaptive morphology is detailed, and in [14] a complementary overview is presented as well as the latest developments and a brief history of adaptive mathematical morphology.

As pointed out in [14], there are two important aspects of adaptive mathematical morphology to address: (1) how to construct adaptive structuring elements which are suitable for the image analysis task, and (2) how to properly define morphological operators with adaptive structuring elements. Among the methods of adaptive morphology, those based on an orientation vector field to adapt the shape and orientation of structuring elements show good ability to preserve the structures of image. The approach followed in this work for constructing the proposed adaptive morphological operators is therefore based on adaptivity with respect to "the spatial neighborhood position" or "gray level image values", which is referred as input-adaptive mathematical morphology by Roerdink [12]. This category of adaptiveness is defined as adaptability with respect to the image content, i.e. the position in the image domain as well as values in the image range. Well founded examples of input-adaptive processing are those based on bilateral morphological operators [15].

There are several alternative formulations for adaptive morphological operators. Adaptive morphological operators can be defined using the notion of impulse functions [16], without explicit use of the adjunction property and then the morphological opening and closing are computed directly without resorting to compositions of the erosion and dilation, which corresponds just to spatially-variant counterpart of the opening (9). Here we adopt another formulation based on the composition of adjoint operators in a quite general setting and which is easily used in our case.

In this work, the adaptive structuring elements change their shape and orientation according to the edges of the objects contained in the image by means of an orientation vector field. The orientation vector field is defined in

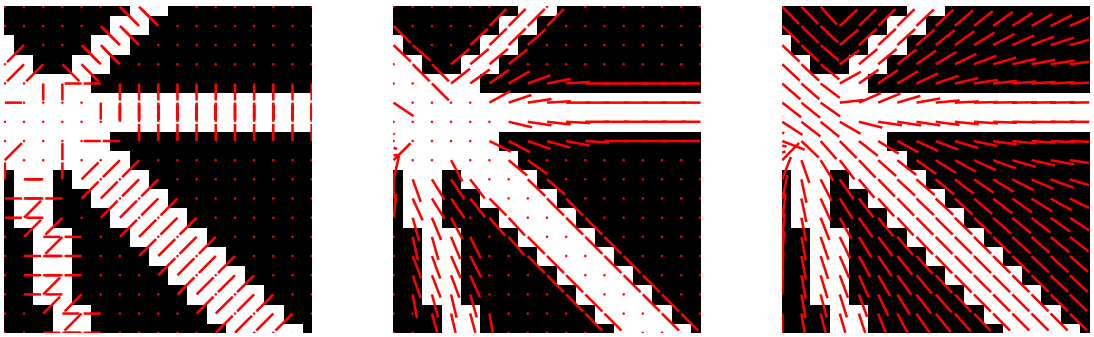

(a) Gradient (b) ASG (c) ASGVF

Figure 1: Single orientation vector fields (SOVF): a) image gradient, b) average squared gradient (ASG) [19], c) average squared gradient vector flow (ASGVF) [20].

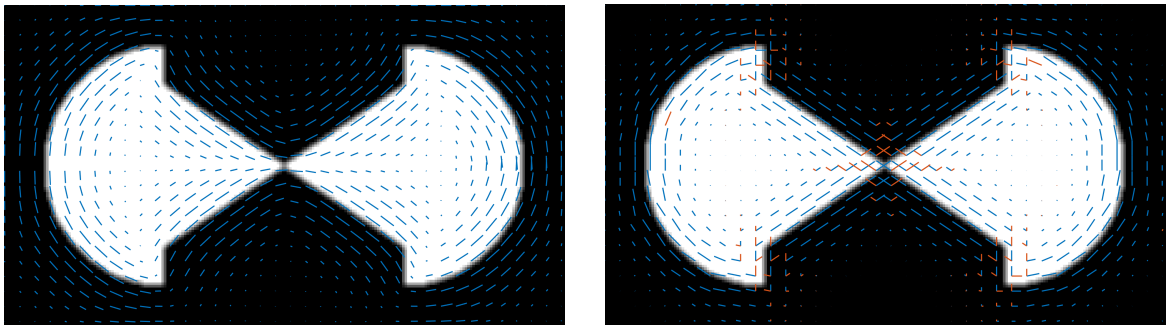

(a) Single orientation vector field (b) Multiple orientation vector field

Figure 2: Comparison of orientation vector fields considering (a) a single orientation or (b) multiple orientations at each pixel. The single orientation vector field has been obtained by the ASGVF method [20] whereas the multiple orientation vector field has been obtained by the method described in Section 2.1.

all pixels of the image and can provide only one orientation at each pixel (single orientation estimation methods) or the main orientations existing at that pixel (multiple orientation estimation methods). The first group of methods shows excellent performance in scenarios where there is only one dominant orientation but does not consider that a pixel may have associated several predominant orientations, as crossing lines (X-junction), corners (L-junctions) and junctions (Y-junctions) [17]. These methods are usually based on the image gradient and provide the orientation by averaging its values. Some of these methods are, e.g., the local structure tensor (LST) [17], principal component analysis (PCA) [18], the average squared gradient (ASG) [19] and its regularization, the average squared gradient vector flow (ASGVF) [20]. For sake of clarity, some of them are shown in Fig.1. Note that the LST method, PCA method and the ASG method provide equivalent single orientation vector fields [21].

The second group of orientation estimation methods considers more than one orientation existing at each pixel. These methods are mainly based on a bank of filters, see, e.g. [22, 23, 24]. A visual comparison between single orientation and multiple orientation estimation method can be observed in Fig.2. It is important to note that the orientation provided by single orientation estimation methods is the local average of the orientations existing at each pixel of the image. On the other hand, multiple orientation estimation methods deal independently each one of the existing orientations, since these methods are more complex and can model this situation.

The aim of this paper is to provide adaptive morphological filters whose structuring elements are spatially-variant based on the information given by a multiple orientation vector field. To this end, the paper is organized as follows:

after this introduction, Section 2 contains the theoretical part of the paper. Firstly, in Section 2.1 the proposed framework to estimate multiple orientations is detailed. Then, in Section 2.2, spatially-variant morphological operators are formulated in the general case, and in Section 2.3, when flat adaptive structuring elements are used. Later, Section 2.4 addresses the definition of the spatially-variant adaptive structuring elements proposed in this work. We also formulate the corresponding metric structuring function and the Hamilton–Jacobi PDE associated to those operators. Results of the proposed filters are shown in Section 3, as well as the comparison with morphological bilateral operators and filters based on a single orientation vector field. Finally, Section 4 closes the paper with the conclusions.

2. Methodology

2.1. Multiple orientation estimation framework

The orientation vector field considered in this work is based on a decomposition of the information of the contours by a bank of orientated linear openings, as shown in Fig.3. Let $f(x) : E \to \mathbb{R}$ be a gray-level image, where the support space is $E \subset \mathbb{Z}^2$ and the pixel coordinates are given by $x \in E$. The edges of the objects in $f(x)$ are provided in $g(x)$ by an edge detector method (e.g. thresholded gradient [25] or Canny method [26]).

The contours are then decomposed by means of a bank of filters. In our approach, these filters are directional openings $\gamma_{L^{\theta_i,l}}$ [1]. The directional opening of $g(x)$ by a linear and symmetric structuring element (SE) of length l and direction θ_i, $L^{\theta_i,l}$, is defined as the directional erosion of g by $L^{\theta_i,l}$ followed by the directional dilation with the same flat structuring element:

$$\gamma_{L^{\theta_i,l}}(g)(x) = \delta_{L^{\theta_i,l}}\left(\varepsilon_{L^{\theta_i,l}}(g)\right)(x), \tag{16}$$

where the definitions of the directional erosion and dilation of f by $L^{\theta_i,l}$ are, respectively,

$$\varepsilon_{L^{\theta_i,l}}(f)(x) = \bigwedge_{h \in L^{\theta_i,l}} \{f(x+h)\}, \tag{17}$$

$$\delta_{L^{\theta_i,l}}(f)(x) = \bigvee_{h \in L^{\theta_i,l}} \{f(x-h)\}. \tag{18}$$

The proposed orientation model is based on a decomposition of the contour information by families of linear openings, $\{\gamma_{L^{\theta_i,l}}\}_{i\in I}$, according to a particular discretization of the orientation space $\{\theta_i\}_{i\in I}$. In the next step of the proposed method, a filtering is performed at each one of the directional openings (depicted as H_σ in Figure 3). The filtering extends the orientation information and reduces angle mismatches due to noise. The kernel H_σ is the sampling of a Gaussian low-pass filter, where σ is the spatial standard deviation of the filter.

Once the directional openings have been filtered, the directional signature at pixel x is defined as the gathering of all responses $\tilde{g}_{\theta_i}(x)$, i.e.,

$$s_{x;l}(i) = \tilde{g}_{\theta_i}(x), \tag{19}$$

providing at each pixel an unidimensional signal over the discrete angles θ_i. Then, in order to determine its peaks, $s_{x;l}(i)$ is interpolated using cubic b-splines [27]:

$$\hat{s}_{x;l}(\theta) = \sum_{i=1}^{N} s_{x;l}(i)\, b_3(\theta - \theta_i), \tag{20}$$

$\hat{s}_{x;l}(\theta)$ becoming a continuous and differentiable signal and θ being a continuous variable denoting the angle. Note that we are interested in the orientation of the contours and not in the direction, this is achieved by the symmetry of the orientated structuring elements used in the openings, consequently $\hat{s}_{x;l}(\theta)$ is a periodic signal, whose period is 180 degrees. The peaks of $\hat{s}_{x;l}(\theta)$ are found by searching the angles θ_p where the first derivative equals zero and checking that the second derivative is negative at these angles. Only those angles θ_p whose peak value is greater than a given threshold will be considered. These maxima correspond to the multiple orientations existing at pixel x. Finally, collecting all the orientations estimated at all the pixels in the image provides the multidimensional vector field $\vec{\theta}(x)$.

Figure 4 shows the images and signals involved in the multiple orientation estimation framework. In this visual example, the length of the orientated linear structuring element is $l = 9$. When dealing with discrete images, it is

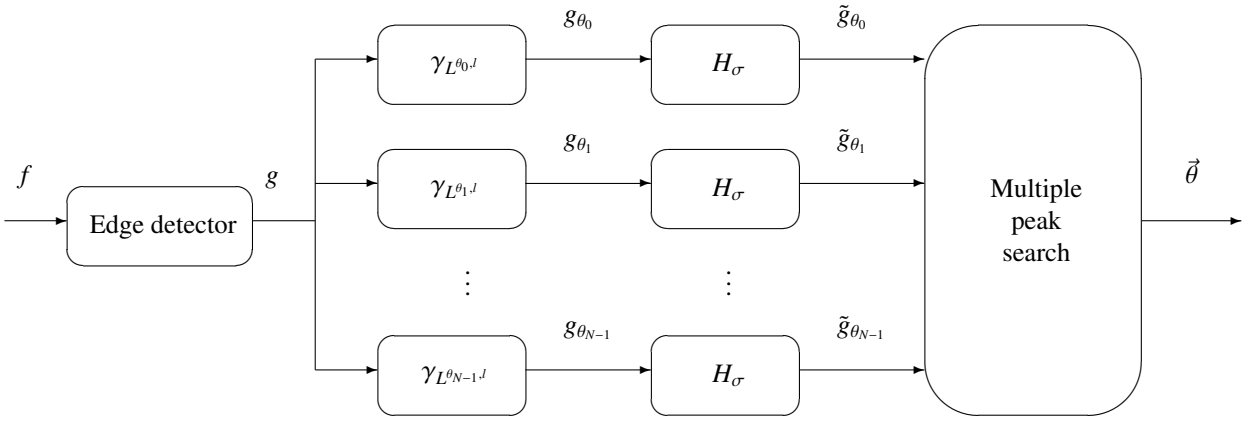

Figure 3: Block diagram of the multiple orientation estimation framework.

important to remember the effects of discretization. As described in [20], the angular resolution of a structuring element of length l is $\Delta_\theta = \frac{90}{l-1}$ degrees, therefore the angles that can be used are $\theta_i = i\,\Delta_\theta$, $i \in I = [0, N-1]$, with $N = 2(l-1)$. It is important to remark that a long structuring element allows for a larger angular resolution (i.e., more directions) but the structures to be detected have to be bigger. On the other hand, a smaller structuring element offers fewer directions but it allows get into small details in the image. In this example, the number of branches in the bank filter is $N = 16$, the angular resolution is $\Delta_\theta = 11.25$ degrees and the spatial standard deviation of the Gaussian low-pass filter is $\sigma = 5$. Fig. 4(z)-Fig.4(ab) show the directional signature for three selected pixels in Fig. 4(a), where the detected maxima in the directional signature correspond to the multiple orientations existing at those pixels.

2.2. Abstract formulation for spatially-variant morphological operators

As discussed above, morphological operators are classically defined for images supported on Euclidean spaces. Recent works have extended mathematical morphology for real valued images whose support space is a Riemannian manifold [28], or more generally, a length space [29, 30]. Let us introduce a formulation which is compatible with Euclidean, Riemannian and length-space settings as well as with the adaptive approach of structuring elements. This abstract setting is based on the theory max-plus mathematics (also known as idempotent analysis [31, 32, 33]).

Metric Maslov measure space. The theoretical foundations of Maslov idempotent measure theory [32] are based on replacing in the structural axioms of probability theory the role of the classical semiring $\mathrm{S}_{(+,\times)} = (\mathbb{R}_+, +, \times, 0, 1, \leq)$ of positive real numbers by the idempotent semiring: $\mathrm{S}_{(\max,+)} = (\bar{\mathbb{R}}, \max, +, -\infty, 0, \leq)$. In this context, a change of the measure involves a consistent counterpart to the standard probability theory.

Let (X, d) be a (Hausdorff topological) metric space and let $\mathfrak{m}$ be a Maslov idempotent measure on X, i.e., mapping from X in the max-plus semiring such that for every function $f : X \to \bar{\mathbb{R}}$, we have $A \subset X$,

$$\mathfrak{m}_f(A) = \sup_{x \in A} f(x). \tag{21}$$

The triple $(X, d, \mathfrak{m})$ is called a metric Maslov measure space.

Admissible structuring function. A Maslov idempotent measurable function $\mathfrak{b} : X \times X \to \bar{\mathbb{R}}$ defined in $(X, d, \mathfrak{m})$ is said to be an admissible structuring function if the following conditions are satisfied $\forall x, y \in X$,

- Nonpositivity and total mass inequality:

$$\mathfrak{m}\left(\mathfrak{b}(x, \cdot)\right) = \sup_{y \in X} \mathfrak{b}(x, y) \leq 0 \Leftrightarrow \mathfrak{b}(x, y) \leq 0. \tag{22}$$

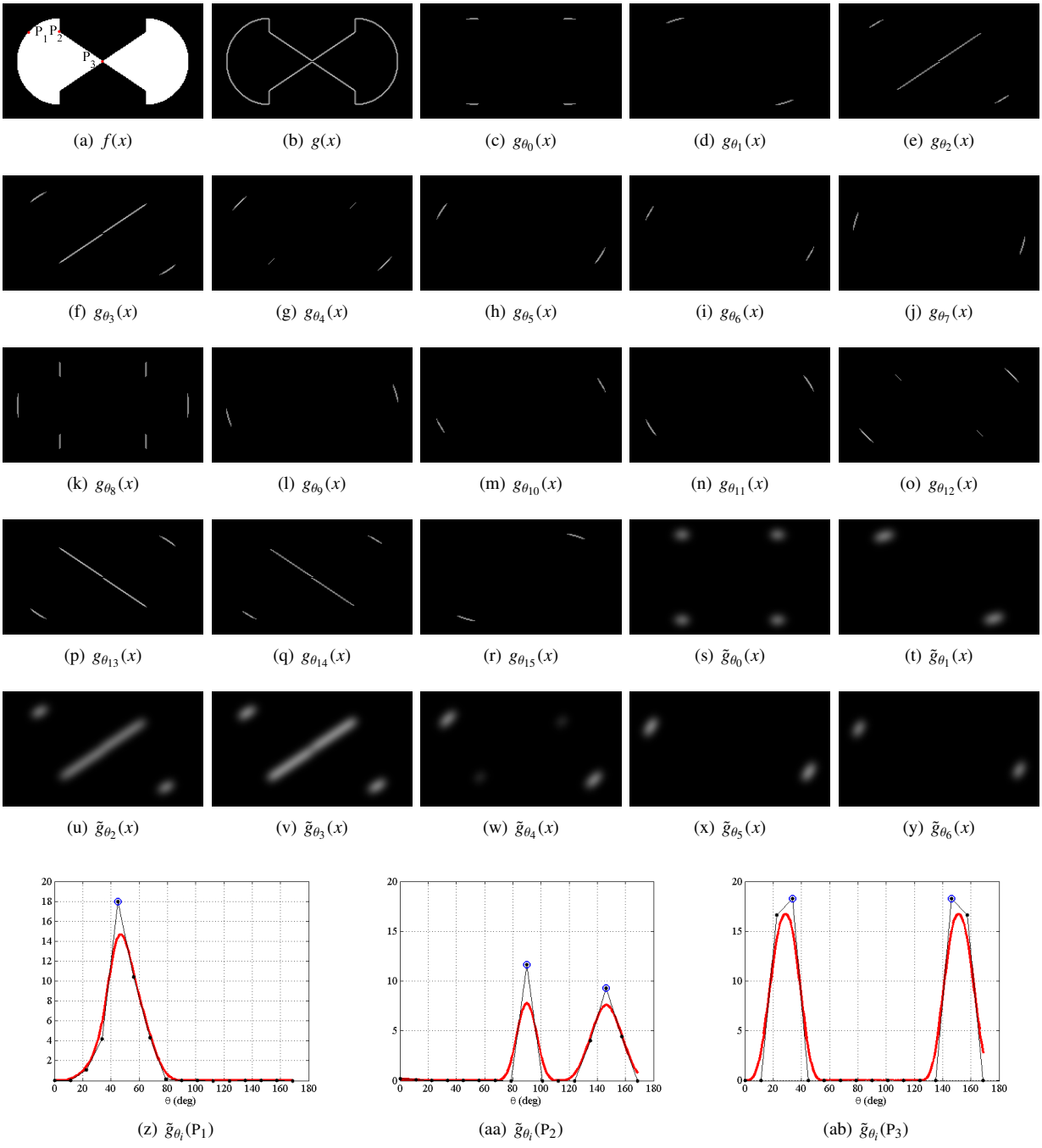

(a) $f(x)$ (b) $g(x)$ (c) $g_{\theta_0}(x)$ (d) $g_{\theta_1}(x)$ (e) $g_{\theta_2}(x)$

(f) $g_{\theta_3}(x)$ (g) $g_{\theta_4}(x)$ (h) $g_{\theta_5}(x)$ (i) $g_{\theta_6}(x)$ (j) $g_{\theta_7}(x)$

(k) $g_{\theta_8}(x)$ (l) $g_{\theta_9}(x)$ (m) $g_{\theta_{10}}(x)$ (n) $g_{\theta_{11}}(x)$ (o) $g_{\theta_{12}}(x)$

(p) $g_{\theta_{13}}(x)$ (q) $g_{\theta_{14}}(x)$ (r) $g_{\theta_{15}}(x)$ (s) $\tilde{g}_{\theta_0}(x)$ (t) $\tilde{g}_{\theta_1}(x)$

(u) $\tilde{g}_{\theta_2}(x)$ (v) $\tilde{g}_{\theta_3}(x)$ (w) $\tilde{g}_{\theta_4}(x)$ (x) $\tilde{g}_{\theta_5}(x)$ (y) $\tilde{g}_{\theta_6}(x)$

(z) $\tilde{g}_{\theta_i}(\mathrm{P}_1)$ (aa) $\tilde{g}_{\theta_i}(\mathrm{P}_2)$ (ab) $\tilde{g}_{\theta_i}(\mathrm{P}_3)$

Figure 4: Estimation of the multiple orientation vector field. (a) Input image $f(x)$, (b) contours of the input image given by the absolute value of the gradient, Fig. 4(c) - Fig. 4(r) g_{θ_i} with the decomposition of the contours by directional openings using an orientated linear structuring element of length $l = 9$. The value of l determines the number of branches, $N = 16$, and the angular resolution, $\Delta_\theta = 11.25$ degrees. Fig. 4(s) - Fig. 4(y) show some of the low-pass filtered images $\tilde{g}_{\theta_i}$ for illustrative purposes. Fig. 4(z) - Fig. 4(ab) show the directional signature of three selected pixels P_1, P_2 and P_3 depicted in Fig. 4(a) with a red dot. The values of $s_{\mathrm{P}_j;l}(i)$, $j = [1, 2, 3]$, are plotted with dots whereas the interpolated signals $\hat{s}_{\mathrm{P}_j;l}(\theta)$ are plotted with continuous red lines. The detected maxima, which correspond to the multiple orientations existing at those pixels, are depicted with blue circles. The threshold considered to decide if a peak is a maximum is the 50% of the maximum peak value.

- Completeness (or conservative):

$$\mathfrak{m}\left(\mathfrak{b}(x,x)\right) = 0 \Leftrightarrow \mathfrak{b}(x,x) = 0. \tag{23}$$

This axiomatic formulation of the notion of admissible structuring function provides us the minimal mathematical requirements to use the function in a pair of adjoint dilation and erosion. In fact, as the name implies, the two axioms are the counterpart of those of a heat kernel in a measure metric space.

Dilation and Erosion operators on $(X, d, \mathfrak{m})$**.** We have now the ingredients to introduce the pair of dilation and erosion for any image f according to $\mathfrak{b}$. Given an admissible structuring function $\mathfrak{b}(x, y)$ in $(X, d, \mathfrak{m})$, the dilation and erosion of a function $f : X \to \bar{\mathbb{R}}$ by $\mathfrak{b}$ are given respectively by

$$\delta_{\mathfrak{b}}(f)(x) = \sup_{y\in X}\left\{f(y) + \mathfrak{b}(x,y)\right\}, \tag{24}$$

$$\varepsilon_{\mathfrak{b}}(f)(x) = \inf_{y\in X}\left\{f(y) - \mathfrak{b}(y,x)\right\}. \tag{25}$$

Both operators are increasing. In addition, the non-positivity and completeness of $\mathfrak{b}(x, y)$ imply that the dilation is extensive and commutes with supremum, and the erosion is anti-extensive and commutes with the infimum, i.e., for a family of functions $f_i : X \to \bar{\mathbb{R}}$, $i \in I$, and any admissible structuring function, one has $\forall x \in X$

$$f_i(x) \le \delta_{\mathfrak{b}}(f_i)(x); \quad \text{and} \quad \delta_{\mathfrak{b}}\left(\bigvee_i f_i\right)(x) = \bigvee_i \delta_{\mathfrak{b}}\left(f_i\right)(x),$$

$$f_i(x) \ge \varepsilon_{\mathfrak{b}}(f_i)(x); \quad \text{and} \quad \varepsilon_{\mathfrak{b}}\left(\bigwedge_i f_i\right)(x) = \bigwedge_i \varepsilon_{\mathfrak{b}}\left(f_i\right)(x).$$

The previous properties are naturally required for any dilation and erosion, even if they are unrelated between them. In addition, we can easily check that the pair $(\varepsilon_{\mathfrak{b}}, \delta_{\mathfrak{b}})$, defined with the convention of change of sign in the convolution and symmetric admissible structuring function,

- are dual by involution, i.e., for any function $f(x)$ and $\forall x \in X$, one has that

$$\delta_{\mathfrak{b}}(f)(x) = -\varepsilon_{\mathfrak{b}}(-f)(x);$$

- forms an adjunction, i.e., for any two functions f and g on $(X, d, \mathfrak{m})$, the pair $(\varepsilon_{\mathfrak{b}}, \delta_{\mathfrak{b}})$ satisfy that $\forall x \in X$

$$\delta_{\mathfrak{b}}(f)(x) \le g(x) \Leftrightarrow f(x) \le \varepsilon_{\mathfrak{b}}(g)(x).$$

Consequently, their composition leads to the opening and closing of f according to the admissible structuring function $\mathfrak{b}$, given respectively by:

$$\gamma_{\mathfrak{b}}(f)(x) = \delta_{\mathfrak{b}} \circ \varepsilon_{\mathfrak{b}}(f)(x) = \sup_{z\in X}\inf_{y\in X}\left\{f(y) - \mathfrak{b}(y,z) + \mathfrak{b}(z,x)\right\}, \tag{26}$$

$$\varphi_{\mathfrak{b}}(f)(x) = \varepsilon_{\mathfrak{b}} \circ \delta_{\mathfrak{b}}(f)(x) = \inf_{z\in X}\sup_{y\in X}\left\{f(y) + \mathfrak{b}(z,y) - \mathfrak{b}(x,z)\right\}. \tag{27}$$

More precisely, their construction by adjunction property involves that the opening (26) (resp. the closing (27)) can be again rewritten as a maximal lower envelope of structuring functions (resp. minimal upper envelope of negative symmetric structuring functions), i.e.,

$$\gamma_{\mathfrak{b}}(f) = \bigvee\left\{\mathfrak{b}(x,y) + \alpha \mid (x,y,\alpha) \in X \times X \times \overline{\mathbb{R}},\ \ \mathfrak{b}(x,y) + \alpha \le f\right\}, \tag{28}$$

$$\varphi_{\mathfrak{b}}(f) = \bigwedge\left\{-\mathfrak{b}(y,x) + \alpha \mid (x,y,\alpha) \in X \times X \times \overline{\mathbb{R}},\ \ -\mathfrak{b}(y,x) + \alpha \ge f\right\}, \tag{29}$$

and therefore they are increasing idempotent and anti-extensive (resp. extensive) operators. Remarkably, the symmetry of the admissible structuring function is not a necessary condition for the adjunction. Nevertheless, in the case of symmetry, i.e., $\mathfrak{b}(x, y) = \mathfrak{b}(y, x)$, the formulation is obviously simplified.

2.3. Adaptive flat morphological operators

In the case of adaptive flat morphological operators in the Euclidean space E, the admissible structuring function $\mathfrak{b}(x, y)$ is associated to a space-variant adaptive structuring element, denoted by $\mathcal{A}(x)$. The mapping $\mathcal{A}$ assigns a possibly different subset of E to each point x of space E according to local features of the image, such that the corresponding admissible structuring function is defined as

$$\mathfrak{b}(x, y) = \begin{cases} 0 & \text{if } y \in \mathcal{A}(x), \\ -\infty & \text{if } y \in \mathcal{A}^c(x). \end{cases} \tag{30}$$

Expressions of operators (24) and (25) are therefore simplified to obtain the adaptive flat dilation and erosion of f by $\mathcal{A}(x)$ as follows:

$$\delta_{\mathcal{A}(x)}(f)(x) = \bigvee_{y \in \mathcal{A}^T(x)} f(y), \tag{31}$$

$$\varepsilon_{\mathcal{A}(x)}(f)(x) = \bigwedge_{y \in \mathcal{A}(x)} f(y). \tag{32}$$

where the transposed set $\mathcal{A}^T(x)$ is defined by the relationship

$$y \in \mathcal{A}^T(x) \iff x \in \mathcal{A}(y), \tag{33}$$

or using the admissible structuring function:

$$y \in \mathcal{A}^T(x) \text{ if } b(y, x) = 0.$$

The operators $\delta_{\mathcal{A}(x)}$ and $\varepsilon_{\mathcal{A}}(x)$ are adjunct once the same structuring element mapping $\mathcal{A}(x)$ is used [12]. Hence, the adaptive flat opening and closing can be defined, respectively, as

$$\gamma_{\mathcal{A}(x)}(f) = \left(\delta_{\mathcal{A}(x)} \circ \varepsilon_{\mathcal{A}(x)}\right)(f) = \bigvee \left\{ \mathrm{Cyl}_\alpha(x) \mid \mathrm{Cyl}_\alpha(x) \leq f \right\}, \tag{34}$$

$$\varphi_{\mathcal{A}(x)}(f) = \left(\varepsilon_{\mathcal{A}(x)} \circ \delta_{\mathcal{A}(x)}\right)(f) = \bigwedge \left\{ \mathrm{Cyl}^T_\alpha(x) \mid \mathrm{Cyl}^T_\alpha(x) \geq f \right\}, . \tag{35}$$

where $\mathrm{Cyl}_\alpha(x)$ is a cylinder of base $\mathcal{A}(x)$ and height α and $\mathrm{Cyl}^T_\alpha(x)$ is the complement of a cylinder of base $\mathcal{A}^T(x)$ and height α. In addition, the adjunction property allows us to make up more complex filters by means of combining adaptive openings and closings, providing for instance sequential filters, which have shown excellent results to restore images corrupted by dark and bright artefacts [1]. More precisely, in this paper we used the adaptive close-open filter, i.e.,

$$CO_{\mathcal{A}(x)}(f)(x) = (\varphi_{\mathcal{A}(x)} \circ \gamma_{\mathcal{A}(x)})(f)(x), \tag{36}$$

and the open-close filter, i.e.,

$$OC_{\mathcal{A}(x)}(f)(x) = (\gamma_{\mathcal{A}(x)} \circ \varphi_{\mathcal{A}(x)})(f)(x), \tag{37}$$

which remove small structures while keeping sharp edges of the remaining ones. It is important to remember that the adaptive structuring elements $\mathcal{A}$ are computed in a way that near the edges of structures the image is filtered preserving these edges and minimizing inter-region filtering whereas far from the edges the structuring elements are designed to maximize the intra-region filtering.

2.4. Sets of ellipses as adaptive structuring elements

Let us focus on two-dimensional images: $E \subset \mathbb{R}^2$. We consider in this study an elliptical shape kernel $\mathcal{E}^{\theta,a,b}$ to be used by the proposed spatially-variant adaptive filters. In the case of orientation vector fields that take into account only a single orientation at each pixel, the multiscale structuring element is defined as

$$\mathcal{A}_t(x) = \mathcal{E}^{\theta(x),a_t(x),b_t(x)}, \tag{38}$$

where $\theta(x)$, $a_t(x)$ and $b_t(x)$ are, respectively, the orientation, major semi-axis and minor semi-axis of the ellipse $\mathcal{E}^{\theta,a,b}$ centered at pixel x. The value of $\theta(x)$ is given by the orientation vector field, whereas the values of $a_t(x)$ and $b_t(x)$ can be provided by the absolute value of this vector field or also by the distance to the nearest edge, and a scale parameter t, which is typically related to the size of the semi-axis.

In the case of considering a multiple orientation vector field, the adaptive multi-scale structuring element at pixel x is given by the set union of multiple ellipses of same shape/size

$$\mathcal{A}_t(x) = \bigcup_{1 \le i \le M_x} \mathcal{E}^{\theta_i(x),a_t(x),b_t(x)}, \tag{39}$$

where $\theta_i(x)$ corresponds to each one of the M_x detected orientations at pixel x. Fig. 5 shows an example of an image with structuring elements at some pixels according to previous definitions. In Fig. 5(a) the elliptical structuring elements are provided using the single orientation vector field of Fig.2(a), whereas Fig. 5(b) shows the multiple-elliptical structuring elements considering the proposed multiple orientation vector field (shown in Fig.2(b)).

From the viewpoint of implementation, it is easy to see that the dilation and the erosion by the proposed adaptive structuring elements as the union of a set of ellipses can be computed in parallel for each ellipse and then, combined by supremum or infimum, i.e., from (39),

$$\delta_{\mathcal{A}_t(x)}(f)(x) = \delta_{\bigcup_{i\in M} \mathcal{E}^{\theta_i(x),a_t(x),b_t(x)}}(f)(x) = \bigvee_i \delta_{\mathcal{E}^{\theta_i(x),a_t(x),b_t(x)}}(f)(x), \tag{40}$$

$$\varepsilon_{\mathcal{A}_t(x)}(f)(x) = \varepsilon_{\bigcup_{i\in M} \mathcal{E}^{\theta_i(x),a_t(x),b_t(x)}}(f)(x) = \bigwedge_i \varepsilon_{\mathcal{E}^{\theta_i(x),a_t(x),b_t(x)}}(f)(x). \tag{41}$$

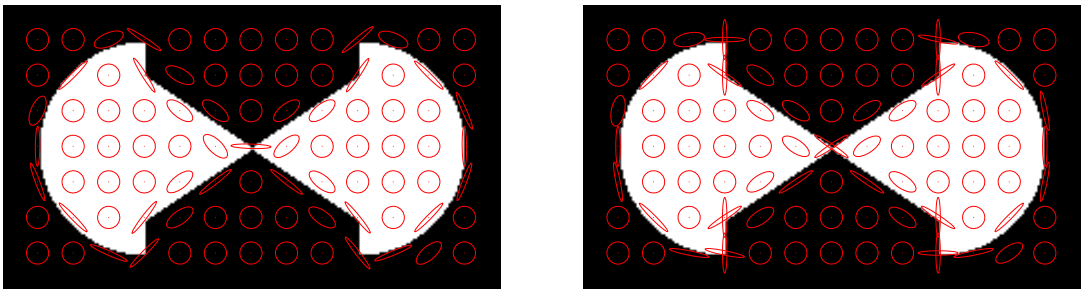

(a) Structuring elements based on SOVF

(b) Structuring elements based on MOVF

Figure 5: Comparison of the elliptical structuring elements $\mathcal{A}_t(x)$ provided by the single orientation vector field (SOVF) of Fig.2(a), and the elliptical structuring elements $\mathcal{A}_t(x)$ provided by the multiple orientation vector field (MOVF) of Fig. 5(b).

2.5. Elliptical structuring functions and metric Hamilton–Jacobi PDE

The previous flat adaptive morphological operators can be related to a family of structuring functions and more theoretically to a metric partial differential equation. The goal of this part is to outline such a preliminary framework which will developed in ongoing work.

Let us initially write the centered ellipse $\mathcal{E}$ in $\mathbb{R}^2$ as the quadratic form

$$\mathcal{E} = \left\{ x \ : \ x^T \mathbf{S} x \le 1 \right\}, \tag{42}$$

where $x \in \mathbb{R}^2$ is the vector referring the coordinate axes and $\mathbf{S}$ is a symmetric positive definite 2×2 matrix, which can be seen as the shape matrix. More precisely, the eigenvalues of $\mathbf{S}$, $\lambda_1 \ge \lambda_2$, are related to the semi-minor and semi-major axes of the ellipse:

$$a = \lambda_2^{-1/2}, \quad b = \lambda_1^{-1/2}; \tag{43}$$

and the angle of the first eigenvector with axis x corresponds to θ in our notation. The ellipse centered at point y is just given by $\left\{x \ : \ (x-y)^T\mathbf{S}(x-y) \leq 1\right\}$. The reader can easily identify the expression of the squared anisotropic Euclidean distance, well known in statistics as the Mahalanobis distance [34]:

$$d_{\boldsymbol{\Sigma}}(x,y) = \sqrt{(x-y)^T\boldsymbol{\Sigma}^{-1}(x-y)}, \tag{44}$$

where the covariance matrix is the inverse of the elliptical shape matrix, i.e., $\boldsymbol{\Sigma} = \mathbf{S}^{-1}$. In other words, each ellipse will provide an anisotropic metric which can be then used similarly to the Euclidean distance in the parabolic structuring function $p_t(x)$. Thus, we introduce the multiscale anisotropic quadratic structuring function of shape $\boldsymbol{\Sigma}$ as:

$$p_{t;\,\boldsymbol{\Sigma}}(x) = -\frac{1}{2t}x^T\boldsymbol{\Sigma}^{-1}x. \tag{45}$$

Because $E \subset \mathbb{R}^2$ endowed with the metric distance $d_{\boldsymbol{\Sigma}}$ is a length space, we may straightforwardly use the theory of morphological PDE on length spaces [29] to this spatially-invariant anisotropic case. First, we introduce the metric subgradient of f at x defined as

$$|\nabla^- f|(x) = \limsup_{y\to x} \frac{[f(y)-f(x)]_-}{d_{\boldsymbol{\Sigma}}(x,y)} = \limsup_{y\to x} \frac{[f(x)-f(y)]_+}{d_{\boldsymbol{\Sigma}}(x,y)}, \tag{46}$$

where $a_+ = \max(a,0)$ and $a_- = \max(-a,0)$. The expression $|\nabla^- f|(x)$ is called descending slope since it measures the downward pointing component of f near x: local variation of f taking into account only values less than $f(x)$. Second, we set the morphological PDE on the metric space $(E, d_{\boldsymbol{\Sigma}})$ as the following initial-value Hamilton–Jacobi first-order equation:

$$\begin{cases} \frac{\partial}{\partial t}u(x,t) \pm \frac{1}{2}|\nabla^- u(x,t)|^2 = 0, \quad \text{in } \ E\times(0,+\infty), \\ \\ u(x,0) = f(x), \quad \text{in } \ E, \end{cases} \tag{47}$$

where the initial condition $f : E \to \mathbb{R}$ is a continuous bounded function. Then, the semigroup solutions of (47) are given by the metric Hopf–Lax–Oleinik formulas [29]:

$$u(x,t) = \sup_{y\in E}\left\{f(y) - \frac{d^2_{\boldsymbol{\Sigma}}(x,y)}{2t}\right\} = (f \oplus p_{t;\,\boldsymbol{\Sigma}})(x) \quad (\text{for} - \text{sign}), \tag{48}$$

$$u(x,t) = \inf_{y\in E}\left\{f(y) + \frac{d^2_{\boldsymbol{\Sigma}}(x,y)}{2t}\right\} = (f \ominus p_{t;\,\boldsymbol{\Sigma}})(x) \quad (\text{for} + \text{sign}). \tag{49}$$

Coming back to our spatially-variant framework, each ellipse i at x involves a scaled local metric associated to the shape matrix $\mathbf{S}(i;x)$:

$$\mathcal{E}^{\theta_i(x),a_i(x),b_i(x)} \mapsto \frac{1}{2t}\mathbf{S}(i;x),$$

in such a way that, associated to the set of ellipses at point x, we can introduce the following admissible structuring function:

$$\mathfrak{p}_t(x,y) = -\frac{1}{2t}\sum_{i=1}^{M_x}(x-y)^T\mathbf{S}(i;x)(x-y). \tag{50}$$

Function $\mathfrak{p}_t(x,y)$ is the counterpart of the flat set $\mathcal{A}_t(x)$ given in (39). Using this admissible structuring function (50), the corresponding adaptive dilation and erosion:

$$\delta_{\mathfrak{p}_t}(f)(x) = \sup_{y\in X}\left\{f(y) - \frac{1}{2t}\sum_{i=1}^{M_x}(x-y)^T\mathbf{S}(i;x)(x-y)\right\}, \tag{51}$$

$$\varepsilon_{\mathfrak{p}_t}(f)(x) = \inf_{y\in X}\left\{f(y) - \frac{1}{2t}\sum_{i=1}^{M_y}(y-x)^T\mathbf{S}(i;y)(y-x)\right\}, \tag{52}$$

lead to anisotropic multiple orientation unflat operators that behave more regularly than the flat ones. In comparison to the spatially-invariant anisotropic case, since at each x the metric is different, i.e., $\mathbf{S}(i;x) \neq \mathbf{S}(i;y)$, the term $(x-y)^T\mathbf{S}(i;x)(x-y)$ lacks of symmetry and therefore does not lead to a distance between x and y. We can nevertheless introduce a local pseudo-metric gradient:

$$|\nabla_x^- f|(x) = \limsup_{y\to x} \frac{[f(y)-f(x)]_-}{\left(\sum_{i=1}^{M_x}(x-y)^T\mathbf{S}(i;x)(x-y)\right)^{1/2}}, \tag{53}$$

which can be used to formulate the following inhomogeneous initial-value first-order differential equation problem:

$$\begin{cases} \frac{\partial}{\partial t}u(x,t) \pm \frac{1}{2}|\nabla_x^- u(x,t)|^2 = 0, & \text{in } E\times(0,+\infty), \\ u(x,0) = f(x), & \text{in } E. \end{cases} \tag{54}$$

There is not a viscous solution of (54) under the form of an analytic expression. However, we conjecture that an appropriate numerical solution of this PDE model can provide significant results.

3. Results

In this section, the proposed spatially-variant adaptive filters based on a multiple orientation vector field (MOVF) are compared to spatially-invariant morphological filters, spatially-variant adaptive filters based on single orientation vector field (SOVF) and adaptive bilateral morphological filters. In order to provide a fair comparison, the different operators are applied to synthetic and real images in several application scenarios.

3.1. Spatially-invariant operators vs spatially-variant operators

Firstly, in order to show the advantages of spatially-variant morphological filters, the spatially-invariant morphological filters are compared to their respective spatially-variant counterparts considering a single orientation vector field (given by the ASGVF [20]) and the multiple orientation vector field described in Section 2.1. The input image used in this comparison is a 256×400 grey level chequerboard pattern. For the spatially-invariant operators, the structuring element b is a disk of 11 pixel of diameter, whereas for the spatially-variant operators the structuring elements $\mathcal{A}(x)$ are based on ellipses which change their shape and orientation according to the orientation vector field. Specifically, the elliptical adaptive structuring elements $\mathcal{E}^{\theta(x),a(x),b(x)}$ are designed as follows: the major semi-axis is $a = 11$ pixels long and the minor semi-axis is $b = 1$ pixel long near the edges and the elliptical structuring elements change gradually their eccentricity until both semi-axes are 6 pixels long in homogeneous areas far from the edges. On the other hand, the operators based on the multiple orientation vector field use the same elliptical function but the adaptive structuring elements are formed by the union of M single orientated ellipses, where M is the number of main orientations detected at each pixel.

Fig.6 displays the spatially-invariant erosion, dilation, opening and closing as well as the spatially-variant counterparts provided by a single and a multiple orientation vector field. The first row shows some structuring elements which are orientated according to the respective vector fields. Fig.6(d)-(f) show the erosion obtained by each structuring element (invariant, based on a single orientation and based on multiple orientations). Fig.6(g)-(i) show the analogue results for dilation. Fig. 6(j)-(l) and Fig. 6(m)-(o) show, respectively, the openings and closings. According to the results, the spatially-invariant operators can not preserve the image structures since the structuring elements always keep the same shape and orientation. The spatially-variant operators based on a single orientation show good results preserving the contours with only one associated orientation but these operators fail when the contours possess multiple orientation like corners or bifurcations. Finally, the spatially-variant operators based on the multiple orientation vector field preserve the image structures in corners, crossing lines and junctions better than operators based on a single orientation because the structuring elements can adapt to these situations with multiple orientations.

		PSNR(dB)	SSIM(%)
	Input Noisy image	18.23	68.75
Close-Open filter: $CO_{\mathcal{A}(x)}(f)(x)$	SOVF	18.41	63.59
	Bilateral	18.30	63.50
	Proposed MOVF	20.91	77.42
Open-Close filter: $OC_{\mathcal{A}(x)}(f)(x)$	SOVF	20.14	67.07
	Bilateral	20.20	70.11
	Proposed MOVF	21.39	76.66
AAF: $\Xi_{\mathcal{A}(x)}(f)(x)$	SOVF	20.72	70.38
	Bilateral	20.94	71.84
	Proposed MOVF	22.48	80.66

Table 1: Quantitative analysis in term of PSNR [40] and SSIM [41] of the visual outcomes in Fig. 7 considering Gaussian noise. This analysis compares adaptive morphological filters based on a single orientation vector fields (SOVF), morphological bilateral filters and adaptive morphological filters based on a multiple orientation vector field (MOVF).

3.2. Spatially-variant morphology in denoising applications

In this comparison, the spatially-variant operators are studied in a denoising application. The aim is to evaluate the ability of these operators to reduce the noise while preserving the image contours. The spatially-variant approaches used in this comparison are: spatially-variant operators using the local structure tensor (LST) [35], spatially-variant operators based on the multiple orientation vector field (MOVF) as was obtained in Section 2.1, and adaptive morphological bilateral filters [15]. The structuring elements used by the operators based on LST and MOVF are the same that were used in the previous comparison. The bilateral approach uses a structuring element based on a disk of 11 pixel of diameter. The filters evaluated are the adaptive sequential morphological filter formed by a closing followed by an opening $CO_{\mathcal{A}(x)}(f)(x)$, the adaptive sequential filter formed by a opening followed by an closing $OC_{\mathcal{A}(x)}(f)(x)$ and the average of the previous operators, the averaged alternate filter (AAF), $\Xi_{\mathcal{A}_{(x)}}(f)(x)$, which presents skilful properties to remove Gaussian and impulsive noise [36]. These filters use predefined shapes as structuring elements unlike other methods, as i.e. general adaptive neighbourhoods [37] or morphological amoebas [38], which impose less restrictions on the shape of the structuring elements. Note that the proposed filters for image denoising are non iterative, unlike, e.g. anisotropic diffusion [39], based on the iterative approximation of the solution of a PDE.

Figure 7 shows the visual outcomes of this comparison in a scenario with Gaussian noise. The input image is a 194×152 real image of a building corrupted with Gaussian noise whose variance is $\sigma = 0.01$. Numerical results of this comparison have been gathered in Table 1 in terms of the peak signal-to-noise ratio (PSNR) (see, e.g. [40]) and the structural similarity index (SSIM) [41]. As can be seen, the proposed adaptive filters based on a multiple orientation vector field achieve the best results reducing the image noise while preserving the contours with multiple orientations compared to the space-variant filters based on a single orientation vector field and the morphological bilateral operators. The key of this improvement is the use of a combination of elliptical structuring elements according to the multiple orientations of the image structures.

Figure 8 shows the comparison of spatially-variant operators in a scenario with impulsive noise. The input image is the same as in the previous case, but now the 5% of its pixels has been corrupted by impulsive noise. Table 2 gathers the numerical results in terms of PSNR and SSIM. Once again, the filters based on MOVF provide the best results since the structuring elements based on multiple orientations can adapt their shape much better to the existing edges. As can be seen, the bilateral filters show the poorest results removing impulsive noise.

3.3. Study of the influence of the size of structuring elements on spatially-variant operators

One of the most interesting applications of spatially-variant filters consists in using orientated structuring elements to erode, dilate, remove or link only the image structures with a particular orientation feature. An example of this idea can be found in Figure 9, where orientated closings of different sizes have been used to link elongates structures of a cell image. In addition, the results are compared to invariant and bilateral closings in order to illustrate the advantages of the spatially-variant operator based on the orientations in this kind of applications.

		PSNR(dB)	SSIM(%)
	Input Noisy image	19.01	70.42
Close-Open filter: $CO_{\mathcal{A}(x)}(f)(x)$	SOVF	18.75	70.13
	Bilateral	18.88	65.50
	Proposed MOVF	19.52	77.73
Open-Close filter: $OC_{\mathcal{A}(x)}(f)(x)$	SOVF	19.07	73.33
	Bilateral	28.20	65.11
	Proposed MOVF	19.92	79.37
AAF: $\Xi_{\mathcal{A}(x)}(f)(x)$	SOVF	21.85	74.94
	Bilateral	20.94	71.84
	Proposed MOVF	22.96	81.45

Table 2: Quantitative analysis in term of PSNR [40] and SSIM [41] of the visual outcomes in Fig. 8 considering impulsive noise. This analysis compares adaptive morphological filters based on a single orientation vector fields (SOVF), morphological bilateral filters and adaptive morphological filters based on a multiple orientation vector field (MOVF).

The first row of Figure 9 shows an invariant closing with circular structuring elements of $r = 6$ pixels of radius, a bilateral closing based on circular structuring elements of $r = 6$ pixels of radius and a spatially-variant closing based on MOVF with elliptical structuring element of $a = b = 6$ pixels of major and minor semi-axis in homogeneous areas and $a = 6$ pixel of major semi-axis and $b = 2$ pixel of minor semi-axis near the image structures. The second row shows an invariant closing and a bilateral closing with circular structuring elements of $r = 12$ pixels and an orientated closing with elliptical structuring elements of $a = b = 12$ pixels in homogeneous areas and $a = 12$, $b = 2$ in pixels belonging to the image structures. Finally, the third row displays invariant and bilateral closings with circular structuring elements of $r = 18$ pixels and an orientated closing with elliptical structuring elements of $a = b = 18$ pixels in homogeneous areas and $a = 18$, $b = 2$ in image structures. As observed in Fig.9, the invariant and bilateral openings can not adapt to the image contours yielding deformations in the elongated structures. On the other hand, the closing based on MOVF can adapt much better to the elongated objects preserving the structures and removing the discontinuities.

4. Conclusions

This work has presented a novel formulation and implementation of adaptive spatially-variant morphological filters. The proposed filters use a multiple orientation vector field to adapt the shape and orientation of the structuring elements to the image structures. The numerical and visual outcomes show the excellent performances of the proposed filters and illustrate the ability of the proposed spatially-variant filters to reduce artefacts and noise in images while the main structures with multiple orientation (e.g. bifurcation, crossover or junctions) are preserved.

References

[1] P. Soille, Morphological Image Analysis: Principles and Applications, 2nd Edition, Springer-Verlag, 2003.

[2] J. Serra, Image Analysis and Mathematical Morphology: Theoretical Advances, Vol. II, Academic Press, London, 1988.

[3] H. Heijmans, Morphological Image Operators, Advances in electronics and electron physics: Supplements, Academic Press, 1994.

[4] P. Maragos, Slope transforms: theory and application to nonlinear signal processing, IEEE Transactions on Signal Processing 43 (4) (1995) 864–877. doi:10.1109/78.376839.

[5] R. van den Boomgaard, L. Dorst, Gaussian Scale-Space Theory, Springer Netherlands, 1997, Ch. The Morphological Equivalent of Gaussian Scale-Space, pp. 203–220.

[6] L. Alvarez, F. Guichard, P. L. Lions, J. M. Morel, Axioms and fundamental equations of image processing, Archive for Rational Mechanics and Analysis 123 (3) (1993) 199–257.

[7] P. Maragos, Differential morphology and image processing, IEEE Trans. Image Processing 5 (6) (1996) 922–937. doi:10.1109/83.503909.

[8] M. G. Crandall, H. Ishii, P.-L. Lions, User?s guide to viscosity solutions of second order partial differential equations, Bulletin of the American Mathematical Society 27 (1) (1992) 1–67.

[9] E. Barron, R. Jensen, W. Liu, Hopf–lax–type formula for $u_t + h(u, du) = 0$, Journal of Differential Equations 126 (1) (1996) 48 – 61.

[10] E. H. Diop, J. Angulo, Multiscale image analysis based on robust and adaptive morphological scale-spaces, Image Analysis and Stereology 34 (1) (2014) 39–50. doi:10.5566/ias.993.
[11] L. Najman, H. Talbot (Eds.), Mathematical Morphology: From Theory to Applications, John Wiley & Sons, Inc., Hoboken, NJ, USA, 2013.
[12] J. Roerdink, Adaptivity and group invariance in mathematical morphology, in: Image Processing (ICIP), 2009 16th IEEE International Conference on, 2009, pp. 2253–2256. doi:10.1109/ICIP.2009.5413983.
[13] P. Maragos, C. Vachier, Overview of adaptive morphology: Trends and perspectives, in: Image Processing (ICIP), 2009 16th IEEE International Conference on, 2009, pp. 2241–2244. doi:10.1109/ICIP.2009.5413961.
[14] V. Ćurić, A. Landström, M. J. Thurley, C. L. L. Hendriks, Adaptive mathematical morphology – a survey of the field, Pattern Recognition Letters 47 (0) (2014) 18 – 28. doi:http://dx.doi.org/10.1016/j.patrec.2014.02.022.
[15] J. Angulo, Morphological bilateral filtering, SIAM Journal on Imaging Sciences 6 (3) (2013) 1790–1822.
[16] R. Verdú-Monedero, J. Angulo, J. Serra, Anisotropic morphological filters with spatially-variant structuring elements based on image-dependent gradient fields, IEEE Trans. Image Processing 20 (1) (2011) 200–212.
[17] H. Knutsson, Representing local structure using tensors, Proc. of the 6th Scandinavian Conference of Image Analysis (1989) 244–251.
[18] K. Mardia, P. Jupp, Directional Statistics, Wiley Series in Probability and Statistics, Wiley, 2009.
[19] M. Kass, A. Witkin, Analyzing oriented patterns, Comput. Vision Graph. Image Process. 37 (3) (1987) 362–385.
[20] R. Verdú-Monedero, J. Angulo, Spatially-variant directional mathematical morphology operators based on a diffused average squared gradient field, Lecture Notes in Computer Science: Advanced Concepts for Intelligent Vision Systems 5259 (2008) 542–553.
[21] B. Rieger, L. J. van Vliet, A systematic approach to nd orientation representation, Image and Vision Computing 22 (6) (2004) 453 – 459.
[22] P. Perona, Deformable kernels for early vision, IEEE Transactions on Pattern Analysis and Machine Intelligence 17 (1991) 488–499.
[23] J. Bigün, J. M. H. du Buf, N-folded symmetries by complex moments in gabor space and their application to unsupervised texture segmentation., IEEE Trans. Pattern Anal. Mach. Intell. 16 (1) (1994) 80–87.
[24] E. P. Simoncelli, H. Farid, Steerable wedge filters for local orientation analysis., IEEE Transactions on Image Processing 5 (9) (1996) 1377–1382.
[25] R. C. Gonzalez, R. E. Woods, Digital Image Processing (3rd Edition), Prentice-Hall, Inc., Upper Saddle River, NJ, USA, 2006.
[26] J. Canny, A computational approach to edge detection, IEEE Trans. Pattern Anal. Machine Intell. 8 (6) (1986) 679–698. doi:10.1109/TPAMI.1986.4767851.
[27] M. Unser, A. Aldroubi, M. Eden, B-spline signal processing: Part I - Theory; Part II - Efficient design and applications, IEEE Trans. Signal Processing 41 (2) (1993) 821–848.
[28] J. Angulo, S. Velasco-Forero, Riemannian mathematical morphology, Pattern Recognition Letters 47 (2014) 93–101.
[29] J. Angulo, Proc. of the ISMM'15, 12th International Symposium on Mathematical Morphology and Its Applications to Signal and Image Processing, Springer International Publishing, 2015, Ch. Morphological PDE and Dilation/Erosion Semigroups on Length Spaces, pp. 509–521.
[30] J. Angulo, Proc. of the 5th Int. Conf. on Scale Space and Variational Methods in Computer Vision, Springer International Publishing, 2015, Ch. Morphological Scale-Space Operators for Images Supported on Point Clouds, pp. 78–89.
[31] V. Maslov, Méthodes opératorielles, MIR, 1987.
[32] P. D. Moral, Idempotent Analysis and Its Applications, Vol. 401 of Mathematics and Its Applications, Springer Netherlands, 1997, Ch. Maslov Optimization Theory: Optimality versus Randomness, pp. 243–302.
[33] G. L. Litvinov, V. P. Maslov, G. B. Shpiz, Idempotent functional analysis: An algebraic approach, Mathematical Notes 69 (5) (2001) 696–729.
[34] P. C. Mahalanobis, On the generalised distance in statistics, Proceedings National Institute of Science of India 2 (1) (1936) 49–55.
[35] A. Landström, M. J. Thurley, Adaptive morphology using tensor-based elliptical structuring elements, Pattern Recognition Letters 34 (12) (2013) 1416 – 1422. doi:http://dx.doi.org/10.1016/j.patrec.2013.05.003.
[36] P. Soille, Morphological Image Analysis, Springer-Verlag, 1999.
[37] J. Debayle, J. Pinoli, Spatially adaptive morphological image filtering using intrinsic structuring elements, Image Anal. Sterol. 24 (2005) 145–158.
[38] R. Lerallut, E. Decenciere, F. Meyer, Image filtering using morphological amoebas, Image Vision Comput. 25 (4) (2007) 395–404.
[39] P. Perona, J. Malik, Scale-space and edge detection using anisotropic diffusion, IEEE Trans. Pattern Anal. Machine Intell. 12 (7) (1990) 629–639.
[40] Q. Huynh-Thu, M. Ghanbari, Scope of validity of psnr in image/video quality assessment, Electronics Letters 44 (13) (2008) 800–801.
[41] Z. Wang, A. C. Bovik, H. R. Sheikh, E. P. Simoncelli, Image quality assessment: from error visibility to structural similarity, IEEE Transactions on Image Processing 13 (4) (2004) 600–612.

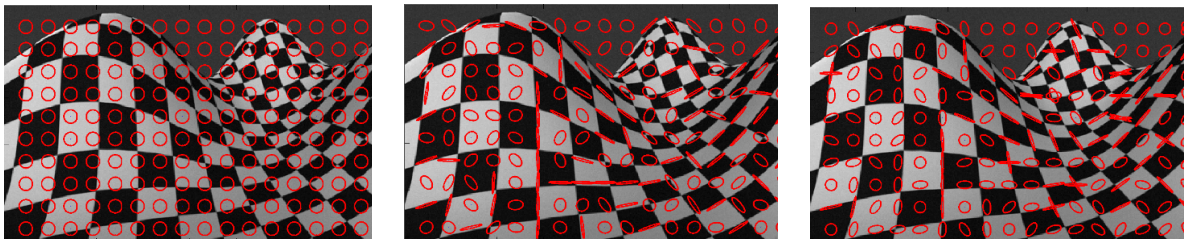

(a) Spatially-invariant SE b (b) Spatially-variant SE $\mathcal{A}(x)$ with SOVF (c) Spatially-variant SE $\mathcal{A}(x)$ with MOVF

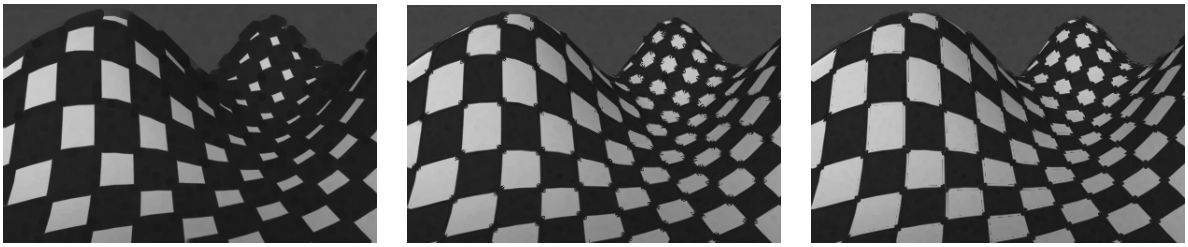

(d) $\varepsilon_b(f)(x)$ (e) $\varepsilon_{\mathcal{A}(x)}(f)(x)$ considering SOVF (f) $\varepsilon_{\mathcal{A}(x)}(f)(x)$ considering MOVF

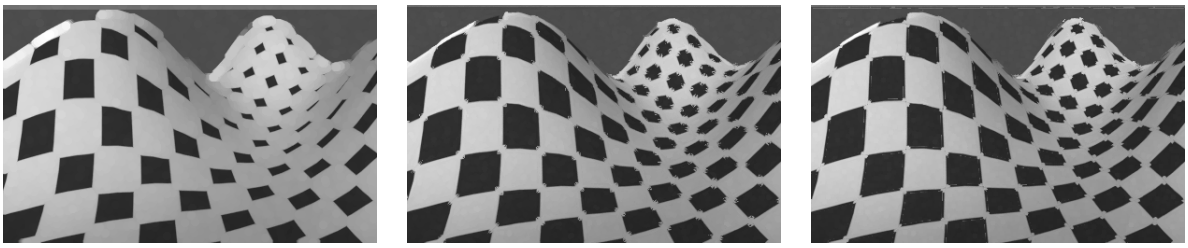

(g) $\delta_b(f)(x)$ (h) $\delta_{\mathcal{A}(x)}(f)(x)$ considering SOVF (i) $\delta_{\mathcal{A}(x)}(f)(x)$ considering MOVF

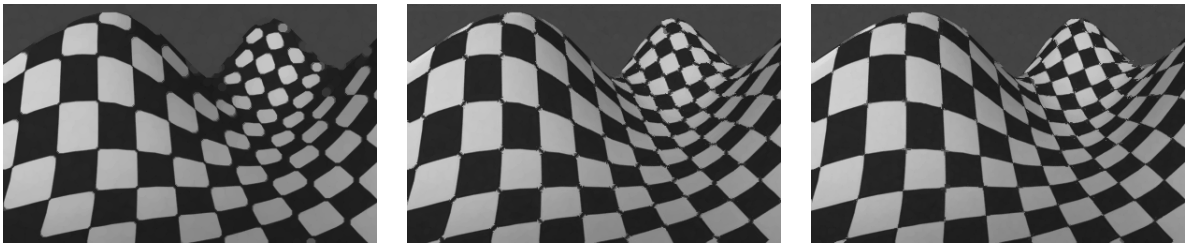

(j) $\gamma_b(f)(x)$ (k) $\gamma_{\mathcal{A}(x)}(f)$ considering SOVF (l) $\gamma_{\mathcal{A}(x)}(f)$ considering MOVF

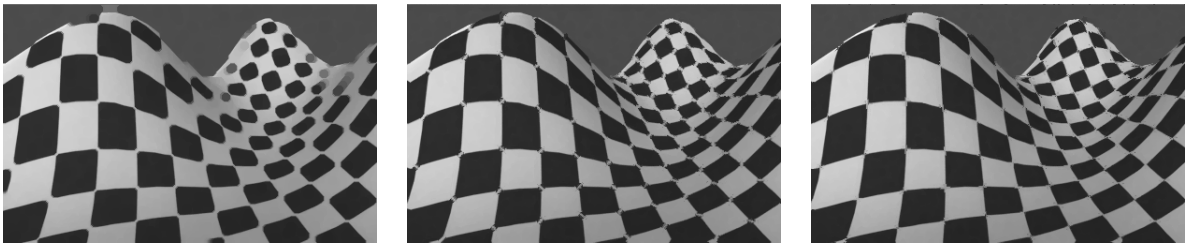

(m) $\varphi_b(f)(x)$ (n) $\varphi_{\mathcal{A}(x)}(f)$ considering SOVF (o) $\varphi_{\mathcal{A}(x)}(f)$ considering MOVF

Figure 6: Comparison of spatially-invariant morphological operators versus their spatially-variant counterparts. First row shows the spatially-invariant structuring element b in (a), the spatially-variant structuring element $\mathcal{A}(x)$ provided by a single orientation vector field in (b), and provided by a multiple orientation vector field in (c). First column contains (d) the spatially-invariant erosion $\varepsilon_b(f)(x)$, (g) dilation $\delta_b(f)(x)$, (j) opening $\gamma_b(f)(x)$ and (m) closing $\varphi_b(f)(x)$. Second and third columns contain (e)-(f) the spatially-variant erosion $\varepsilon_{\mathcal{A}(x)}(f)(x)$, (h)-(i) dilation $\delta_{\mathcal{A}(x)}(f)(x)$, (k)-(l) opening $\gamma_{\mathcal{A}(x)}(f)(x)$ and (n)-(o) closing $\varphi_{\mathcal{A}(x)}(f)(x)$ considering, respectively, single and multiple orientation vector fields.

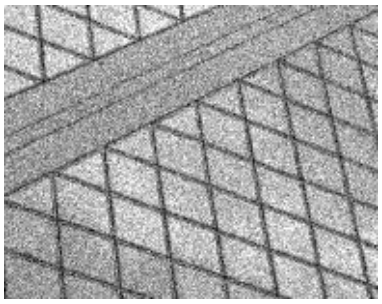

(a) Input image with Gaussian white noise

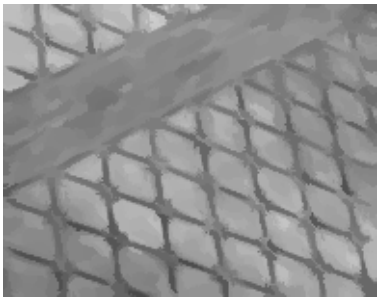

(b) $CO_{\mathcal{A}(x)}(f)(x)$ considering SOVF

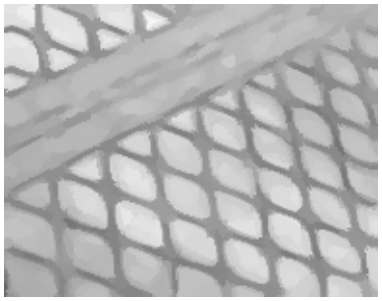

(c) $OC_{\mathcal{A}(x)}(f)(x)$ considering SOVF

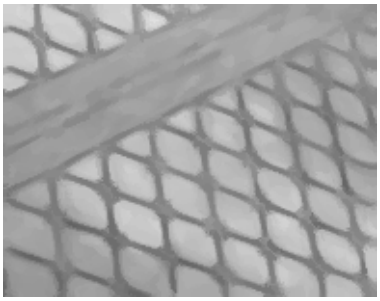

(d) $\Xi_{\mathcal{A}(x)}(f)(x)$ considering SOVF

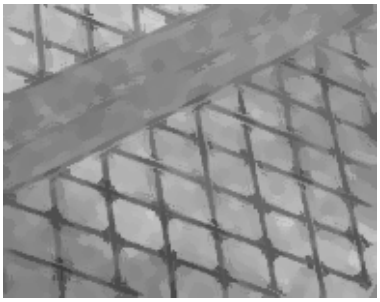

(e) $CO_{\mathcal{A}(x)}(f)(x)$ considering MOVF

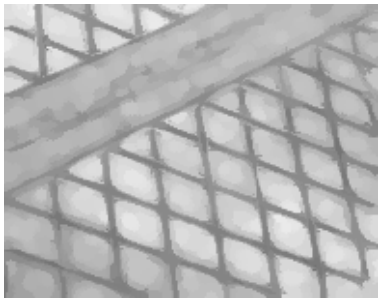

(f) $OC_{\mathcal{A}(x)}(f)(x)$ considering MOVF

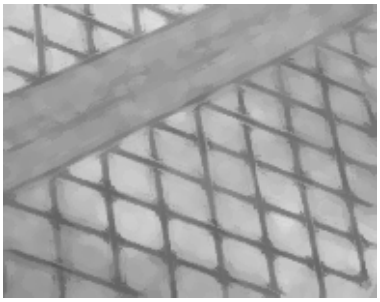

(g) $\Xi_{\mathcal{A}(x)}(f)(x)$ considering MOVF

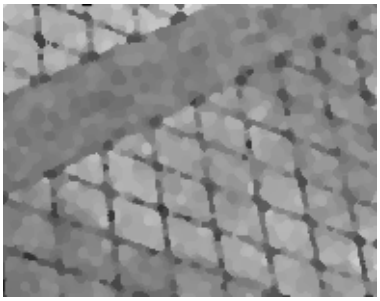

(h) Bilateral $CO_{\mathcal{A}(x)}(f)(x)$

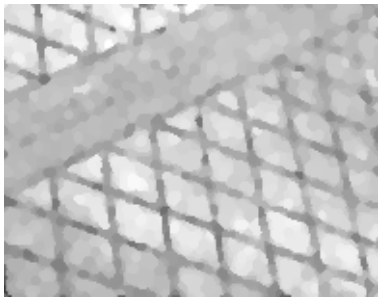

(i) Bilateral $OC_{\mathcal{A}(x)}(f)(x)$

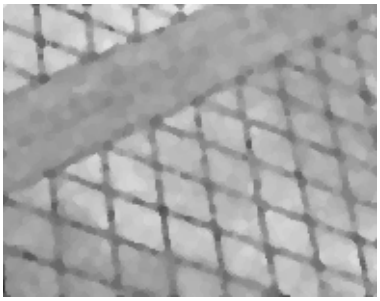

(j) Bilateral $\Xi_{\mathcal{A}(x)}(f)(x)$

Figure 7: Comparison of adaptive morphological filters. The first row shows the input image corrupted with additive white Gaussian noise whose variance is $\sigma = 0.01$. The second row shows the filtered images using operators based on a single orientation vector field (SOVF), the third row contains the output of these filters considering a multiple orientation vector field (MOVF) and the fourth row shows the output of these filters considering the morphological bilateral approach. First column contains the outcomes of the adaptive close-open filter $CO_{\mathcal{A}(x)}(f)(x)$, second column shows the results of the adaptive open-close filter $OC_{\mathcal{A}(x)}(f)(x)$, and third column shows the alternate filter $\Xi_{\mathcal{A}(x)}(f)(x)$.

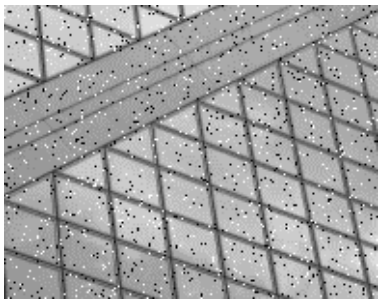

(a) Input image

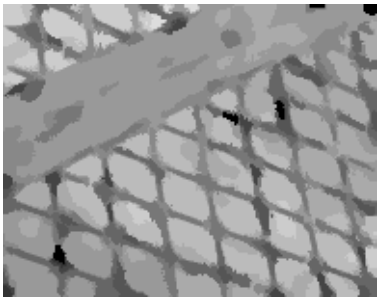

(b) $CO_{\mathcal{A}(x)}(f)(x)$ considering SOVF

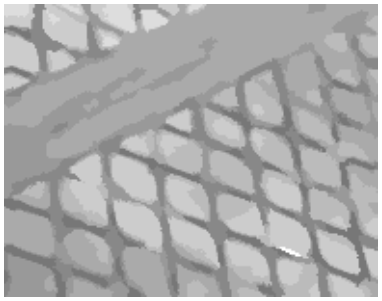

(c) $OC_{\mathcal{A}(x)}(f)(x)$ considering SOVF

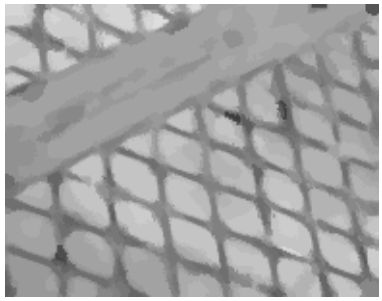

(d) $\Xi_{\mathcal{A}(x)}(f)(x)$ considering SOVF

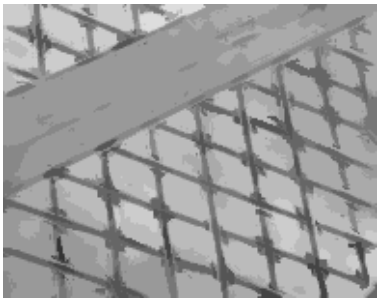

(e) $CO_{\mathcal{A}(x)}(f)(x)$ considering MOVF

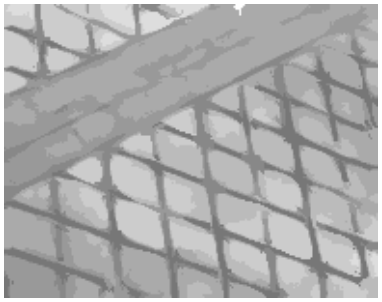

(f) $OC_{\mathcal{A}(x)}(f)(x)$ considering MOVF

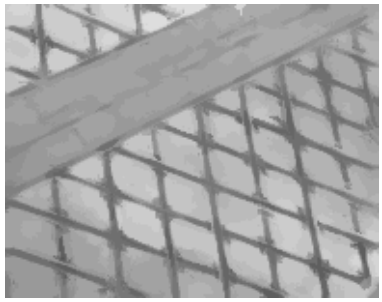

(g) $\Xi_{\mathcal{A}(x)}(f)(x)$ considering MOVF

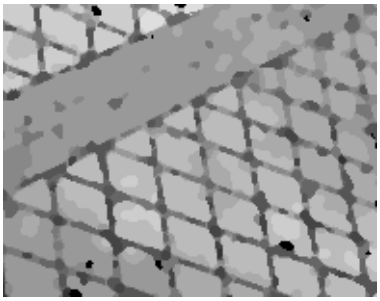

(h) Bilateral $CO_{\mathcal{A}(x)}(f)(x)$

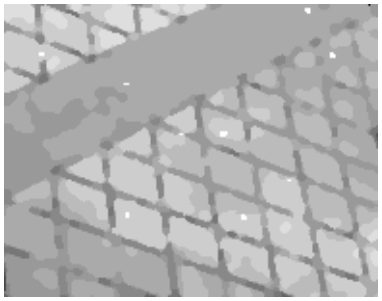

(i) Bilateral $OC_{\mathcal{A}(x)}(f)(x)$

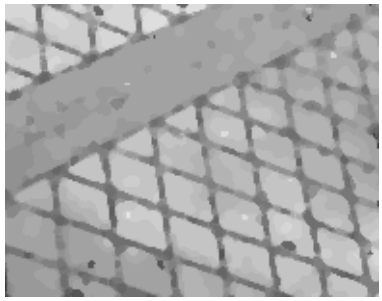

(j) Bilateral $\Xi_{\mathcal{A}(x)}(f)(x)$

Figure 8: Comparison of adaptive morphological filters. The first row shows the input image where the 5% of its pixels has been corrupted by impulsive noise.The second row shows the filtered images using operators based on a single orientation vector field (SOVF), the third row contains the output of these filters considering a multiple orientation vector field (MOVF) and the fourth row shows the output of these filters considering the morphological bilateral approach. First column contains the outcomes of the adaptive close-open filters $CO_{\mathcal{A}(x)}(f)(x)$, second column shows the results of the adaptive open-close filters $OC_{\mathcal{A}(x)}(f)(x)$, and third column shows the alternate filters $\Xi_{\mathcal{A}(x)}(f)(x)$.

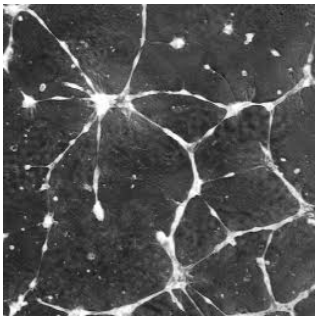

(a) Input image

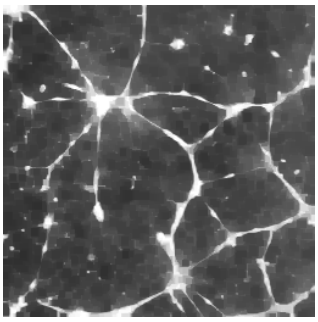

(b) Invariant closing, $r = 6$

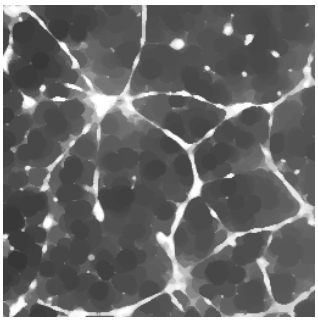

(c) Bilateral Closing

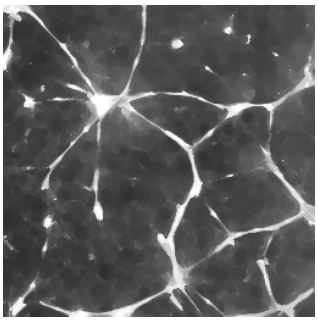

(d) Closing considering MOVF

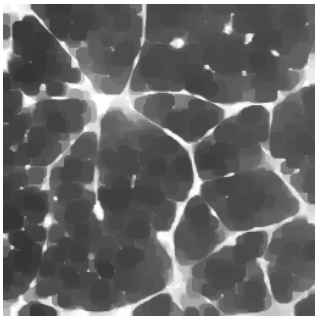

(e) Invariant closing, $r = 12$

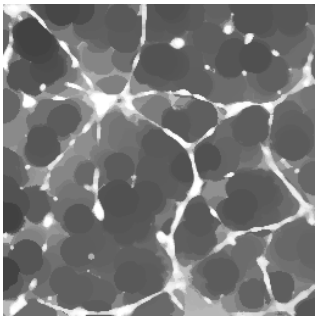

(f) Bilateral Closing

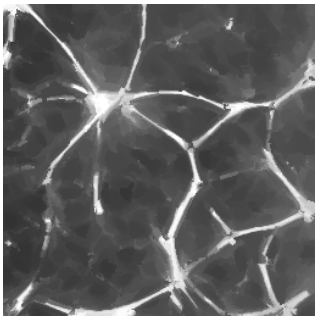

(g) Closing considering MOVF

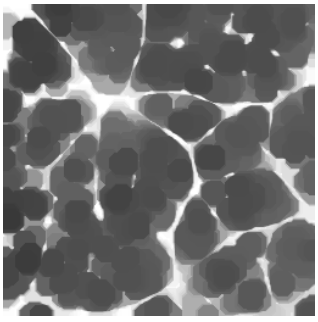

(h) Invariant closing, $r = 18$

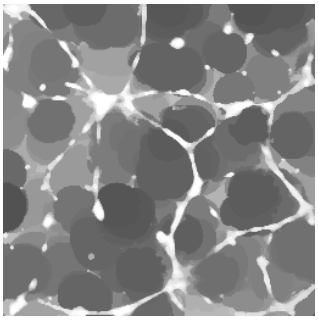

(i) Bilateral Closing

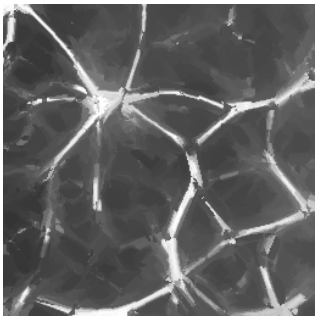

(j) Closing considering MOVF

Figure 9: Comparison of closings with different sizes. (a) Input image: 256×256 gray level image of a cell. First column shows the results of the spatially-invariant closing $\varphi_b(f)(x)$ using disk with radius r equal to (b) 6 pixels, (e) 12 pixels and (h) 18 pixels. The second and third columns show, respectively, the results of the morphological bilateral closings and the spatially-variant closings considering a MOVF (the size of the adaptive structuring elements is detailed for each case in Section 3.3.